Submicron Flow of Polymer Solutions: Slippage Reduction due to Confinement

Amandine Cuenca and Hugues Bodiguel*
Université de Bordeaux, LOF, UMR 5258, F-33600 Pessac, France
CNRS, LOF, UMR 5258, F-33600 Pessac, France
RHODIA, LOF, UMR 5258, F-33600 Pessac, France
(Received 29 October 2012; published 6 March 2013)

Pressure-driven flows of high molecular weight polyacrylamide solutions are examined in nanoslits using fluorescence photobleaching. The effective viscosity of polymer solutions decreases when the channel height decreases below the micron scale. In addition, the apparent slippage of the solutions is characterized macroscopically on similar surfaces. Though slippage can explain qualitatively the effective viscosity reduction, a quantitative comparison shows that the slip length is greatly reduced below the micron scale. This result indicates that chain migration is suppressed in confined geometries.

DOI: 10.1103/PhysRevLett.110.108304 PACS numbers: 47.57.Ng, 47.61.−k, 83.50.Rp, 83.80.Rs

The transport of complex fluids through micro- and nanochannels is important for many applications in various fields, including energy conversion processes [1], nanotechnologies [2], and flows in porous media [3]. In particular, polymer solutions are widely used to control the viscosity of the fluids. The increase in surface-to-volume ratio and the decrease in length scales below the micrometer scale could involve various physical phenomena that affect the flow [4]. Among them, violation of the no-slip boundary condition has been recognized to be very important for polymer solutions even above the micron scale [5,6]. Indeed, the slip length b, defined by the Navier boundary condition at the solid-liquid interface as $b = v_s/\dot{\gamma}_w$ where v_s is the slip velocity at the channel wall and $\dot{\gamma}_w$ the velocity gradient normal to the surface, could be as high as a few micrometers [7]. As a consequence, the flow of polymer solutions in submicrochannels should be dominated by slippage. Such a situation has been investigated in porous media, leading to a decrease in the effective viscosity of the solution (see, for example, Ref. [8]).

The mechanisms responsible for these large slip lengths depend on the concentration regime and the polymer wall adsorption [6,9]. For polymer solutions on nonadsorbing walls, there has been a lot of experimental evidence of the existence of a depletion layer [10–13] close to the wall that is responsible for an apparent slippage. Indeed, in the presence of a thin layer of thickness δ depleted in polymer molecules, it is straightforward to estimate the slip length as $b \approx \delta\eta/\eta_s$, where η and η_s are the solution and solvent viscosity, respectively. The size of this layer has been in debate since the 1980s (see Refs. [5,6], for a review). It could be either of the order of the molecular size (i.e., the radius of gyration R_g in the dilute regime or the correlation length ξ in the entangled regime [14]) or even greater than R_g or ξ [12,15]. Flow-induced migration away from the wall would in the second case explain the large depletion layers that are observed in heterogeneous stress flows, such as capillary ones. This effect could be viewed as a consequence of hydrodynamic forces acting on a deformable object, which are unbalanced if the flow is nonhomogeneous.

During the past decade, this long-lived debate has renewed attention due to the practical importance of transport properties of DNA in nanochannels. Concerning the theoretical part, this subject also benefits from the improvement of several simulation approaches (molecular dynamics, Brownian dynamics, dissipative particle dynamics) [16–22]. In most of these studies, the polymer chains migrate away from the wall. Meanwhile, direct observation of such a migration has been reported by Fang *et al.* [13,23,24]. However, only a qualitative agreement with the models has been found. Moreover, the full understanding of the role of concentration and polymer characteristics (charges, flexibility) on cross-stream migration remains an open question [22].

Recently, some simulations focused on the effect of confinement on this stress-induced migration [25,26]. One of the main results is the observation of a reduction of the migration when decreasing the channel size down to a few radii of gyration. Hydrodynamic interactions between polymer chains and the wall are screened by the presence of an opposite wall [22]. Therefore, the usual assumption that the slip length solely depends on the wall stress would not be valid in nanofluidic channels.

Given the recent progress in nanofluidics [27], it is now possible to confine polymer solutions at these length scales on well-controlled smooth surfaces. Recently, we developed an experimental method to characterize pressure-mean velocity dependence in nanoslits [28]. We reported a reduction of the effective viscosity when the thickness is below a few micrometers. This result is likely to be explained by slippage. In this Letter, we report a direct characterization of the wall slip in much larger channels having similar surfaces, and extend the effective viscosity measurements by varying the concentration, the molecular

weight, and the ionic strength of polyelectrolyte solutions. Such an approach allows us to access indirectly the slippage properties of polymer solutions in channels confined below the micrometer scale.

Materials.—We use several aqueous solutions of partially hydrolyzed polyacrylamide flowing in glass channels (a negatively charged surface that can be considered as nonadsorbent [29]). For two polymer molecular weights of 2×10^5 and 8×10^6 g/mol (referred hereafter as HPAM200k and HPAM8M, purchased from Sigma-Aldrich and obtained from SNF, respectively), the concentration is varied below or of the order of the concentration c_e above which the chains are entangled. Note that, for polyelectrolytes, this concentration is well above the overlap concentration c^* [30]. All solutions are characterized using standard rheometry. The HPAM200k solutions exhibit a Newtonian behavior on the entire range of concentration and shear rate tested, while the HPAM8M ones exhibit a shear-thinning behavior (see Supplemental Material [31]).

Effective viscosity in nanoslits.—Let us first describe the specific setup used to characterize the flow of these solutions in nanoslits.

The experimental device, sketched in Fig. 1, consists in two parallel microchannels, linked by nanoslits series, all etched in glass precisely like the microchannels used for the slip velocity measurements. The microchannels' height varies between 10 and 40 μm, whereas the nanoslits have much lower heights from 180 to 4500 nm. The nanoslits' widths ranges from 10 to 40 μm (the biggest width corresponds to the biggest height). Parallel plate approximation is thus appropriate. The etched glass wafer is bond either to another glass wafer by thermal bonding or to a silicon wafer by anodic bonding [32]. The second procedure is preferred to the first one for the thinnest nanoslits studied since it does not induce a buckling of the channels. The channels' thicknesses are determined through a hydrodynamical calibration [28]. An unbalanced pressure difference is imposed by a pressure regulator (MFCS 4C, Fluigent) at the inlets and outlets of microchannels (see Fig. 1). Since the contribution of the flows in the nanoslits to the ones in the microchannels is negligible, the pressure gradient in the microchannel is uniform. Using the notation of Fig. 1, the pressure drop applied on the ith nanoslit is then simply given by $\Delta P_i = (P_2 - P_1)(L - L_i)/L$.

It is not possible to obtain a z-resolved velocity profile in nanoslits due to their small thickness. However, the mean velocity of the flow is achieved by a time-resolved photobleaching experiment. Briefly, a fluorescent dye, fluorescein isothiocyanate (FITC), is dissolved in the solution at 0.1×10^{-3} mol/L and a line perpendicular to the flow direction is illuminated with a laser beam (488 nm, 100 mW) at a maximum power of 100 mW during 3–5 ms to cause bleaching of the molecules. After this illumination, the channel is imaged at a much lower laser intensity,

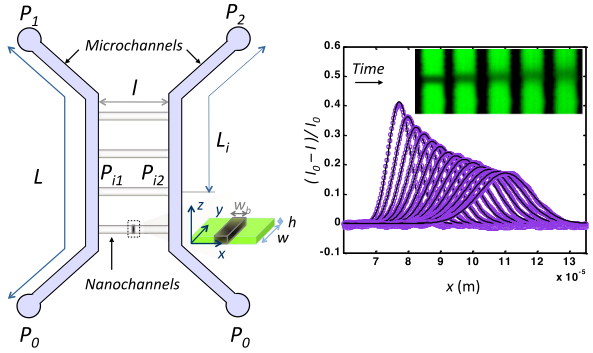

FIG. 1 (color online). Scheme of the microfluidic device and principle of the velocity measurement. Pressure-driven flows are established in nanoslits and imaged after a bleaching procedure. The intensity profiles are fitted with Gaussian functions to extract the mean velocity.

and the displacement of the bleached region is monitored (see Fig. 1). The fluorescence intensity is averaged in the direction perpendicular to the flow and then fitted using Gaussian profiles in order to extract the displacement of the bleached region. Given the small thicknesses investigated and the time scale of the experiments, the fluorescent dye diffuses along the channel height, and the measured velocity v_0 corresponds to the mean velocity. The pressure drop is systematically varied so that the wall shear stress ranges between 0.1 and 20 Pa. These experiments thus lead to a pressure drop/mean velocity relation, which, for Newtonian liquids and no slip at the wall, is simply related to the viscosity of the liquid by $v_0 = h\sigma_w/6\eta$, in the parallel plate approximation. This setup has been validated using various water-glycerol mixtures [28].

We applied this method to several concentrations of the two HPAM used for the slippage measurements. Figure 2 shows some examples of the mean velocity measurements. In all cases, we find a linear dependency with the wall shear stress, even for the solutions of HPAM8M, which exhibits shear-thinning behavior. This is probably due to the fact that the flow at these scales is dominated by slippage, for which we experimentally find a linear dependence with the wall shear stress (see the following section).

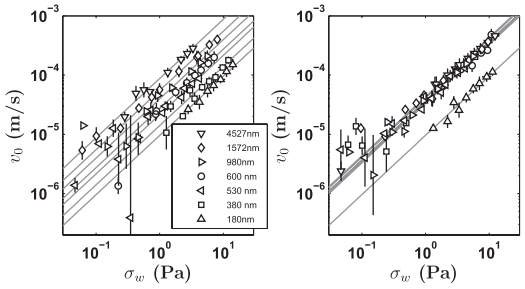

FIG. 2. Examples of mean velocity results in nanoslits of thicknesses from 180 to 4500 nm as a function of the wall shear stress, for HPAM200k at 0.5% (left) and for HPAM8M at 0.1% (right). Each series is fitted by a linear function.

Since it is not possible to dissociate experimentally the slippage at the wall from the shear flow, we analyze these results in terms of an effective viscosity η_{eff}, which would be that of Newtonian fluid with no slip at the wall, i.e., $\eta_{\text{eff}} = h\sigma_w/6v_0$. Figure 3 shows the evolution of the effective viscosity as a function of the channel height. For all the solutions tested, a reduction of the effective viscosity is observed. This reduction is rather high for the most concentrated solutions.

Slippage characterization.—Then, we characterize the slip velocity of the same solutions in a microchannel, where confinement effects should be negligible, by using a z-resolved micro–particle image velocimetry technique. A pressure-driven flow is set up in a large aspect ratio microchannel of height $h = 43$ μm, width 520 μm, and length $l = 48.5$ mm, etched in glass using standard photolithography and wet etching [33]. The solution contains fluorescent tracers of diameter 1 μm (Fluorosphere, purchased from Invitrogen) and the flow is imaged thanks to confocal microscopy. It is usually not easy to accurately measure a slip velocity, mainly due to the fact that the exact distance between the tracers and the wall is not well known. The method used is briefly described below. In order to achieve a satisfying vertical resolution, we combine particle tracking velocimetry and a continuous vertical scan. The acquisition rate is chosen so that a tracer is seen on a few successive frames (typically between 5 and 20). The velocity of the tracer is directly measured through the determination of its successive displacements. Meanwhile, we correlate the fluorescence intensity to the z position of the confocal plane. It is maximum when the confocal plane coincides with the exact location of the tracer. The velocity profile is then obtained by combining the velocities of many tracers and their vertical position. Figure 4 shows some examples of measured profiles. Determination of the slip velocity also requires one to know with a good precision the position of the wall. The latter is obtained thanks to a vertical scan of the device, as the solution also contains a molecular dye: FITC (at 0.1×10^{-3} mol/L purchased from Sigma-Aldrich). The inflection point of the intensity profile is taken to be the position of the surface. This method is validated with several water-glycerol mixtures. A very good agreement with Poiseuille law is found with no slip at the wall, within a typical error of less than 5%.

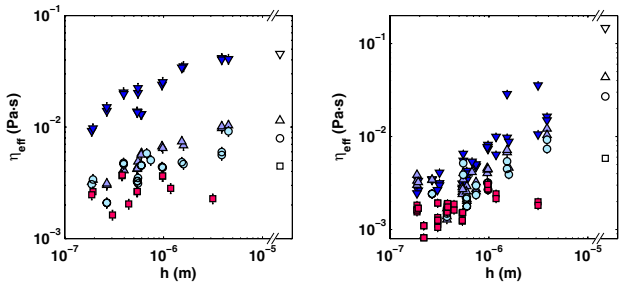

FIG. 3 (color online). Effective viscosity as a function of channel thickness in comparison with bulk viscosities (empty symbols). Left: HPAM200K solutions at 5% (down triangles), 1% (up triangles), 0.5% (circles), 1% + 10 g/L NaCl (squares). Right: HPAM8M solutions at 0.2% (down triangles), 0.1% (up triangles), 0.05% (circles), 0.1% + 10 g/L NaCl (squares).

This method is applied systematically to several polymer solutions, for wall shear stress $\sigma_w = \Delta Ph/2l$ ranging from 0.5 to 50 Pa. The velocity profile allows us to access the viscosity of the solution and we find a good agreement with the one acquired by standard rheometry experiments. We focus here on the slippage velocity. For both polymers, the slip velocity is found to be proportional to the wall stress at first approximation, as shown in Fig. 4. The corresponding slip length $b = v_s\eta/\sigma_w$ ranges from 5 to 15 μm with η the solution viscosity, v_s the slippage velocity, and σ_w the wall shear stress. Note that for the shear-thinning polymer solutions, a reference shear stress of 1 Pa is chosen here and in the following. Interpreting the slippage as a consequence of a depletion layer of thickness $\delta = b\eta_s/\eta$, we find, as shown in Fig. 4, that δ is of the order of a few hundreds of nanometers and decreases when the concentration increases. This order of magnitude is much higher than the correlation length of the polymer solutions tested which ranges between 10 and 50 nm (see Supplemental Material [31]). Since electrostatic interactions should be screened at these length scales (the Debye length is of the order of 1 nm), such a high depletion layer should be due to a flow-induced migration away from wall.

Discussion.—The effective viscosity reduction is likely to be due to the fact that these solutions exhibit a rather large slippage. Indeed, removing the no-slip boundary conditions, we could express the mean velocity as $v_0 = v_s + 6h\sigma_w/\eta$ in the case of a Newtonian liquid. Using the slip length definition $b = \eta v_s/\sigma$, the normalized effective viscosity is given by

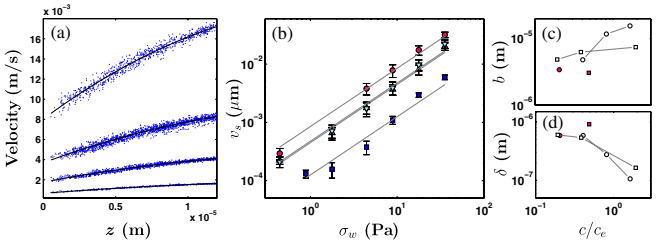

FIG. 4 (color online). (a) Examples of velocity profiles (from the bottom to the top, $\sigma_w = 1.8, 4.4, 8.9, 17.7$ Pa), for solutions of HPAM200k at 1%. Each data point corresponds to a single tracer. The solid lines are the best fit to the data given by $v = v_s + \sigma_w z(h - z)/h\eta$. (b) Slippage velocity as a function of the wall shear stress for HPAM200k solutions of weight fraction 0.5% (down triangles), 1% (up triangles), 5% (squares), and 1% containing 10 g/L NaCl (circles). The solid lines are the best linear fit to the data. (c) Slip length $b = \eta v_s/\sigma$ and (d) thickness of the depletion layer $\delta = b\eta_s/\eta$, plotted as a function of the concentration c/c_e, for solutions HPAM8M (circles) and HPAM200k (squares).

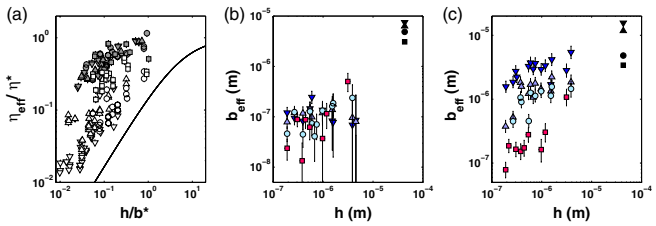

FIG. 5 (color online). (a) Normalized effective viscosity as a function of normalized channel thickness. Filled symbols correspond to HPAM200K solutions, whereas the empty ones correspond to HPAM8M solutions. The solid lines represent the normalized effective viscosity predictions, under the assumption of a macroscopic and constant slippage Eq. (1). (b) Effective slip length as a function of the channel thickness for HPAM200K solutions at 5% (down triangles), 1% (up triangles), 0.5% (circles), 1% + 10 g/L NaCl (squares). Black symbols correspond to the macroscopic direct slip measurements. (c) HPAM8M solutions at 0.2% (down triangles), 0.1% (up triangles), 0.05% (circles), 0.1% + 10 g/L NaCl (squares).

$$\frac{\eta_{\mathrm{eff}}}{\eta^*} = \frac{1}{1 + 6b^*/h}, \tag{1}$$

where $\eta^* = \eta/\alpha$, $b^* = b/\alpha$, and $\alpha = 1$ for a Newtonian fluid. For the shear-thinning solutions that verify $\sigma \propto \dot{\gamma}^n$, we reach a similar expression by fixing the wall shear stress at a constant value of 1 Pa. Only the value of α is changed and equals $3n/(2n + 1)$.

This prediction of the normalized effective viscosity is plotted together with the experimental data in Fig. 5(a), assuming that the slip length is for all thicknesses equal to the one characterized in the large channels and that the viscosity is that of the bulk. For all cases, this prediction is much lower than the measured effective viscosity. Despite the scatter in data, the discrepancy between measurement and prediction suggests that the bulk viscosity increases and/or the slip length decreases with confinement, as compared to the macroscopic values. By comparing the slip velocities directly measured in a microchannel and the mean velocities measured in the nanoslits, we even note that the slip velocity is higher than the mean velocity in nanoslits for a given wall shear stress. This means that the slippage is necessarily reduced in confined geometry.

Although one may wonder whether confinement induces filtration, or enhances shear thinning, these effects would lead to a decrease of an effective viscosity, whereas it is found to be higher than expected. The channel height is always greater than or of the order of the chain size. We thus expect neither a strong filtration [34] nor a great modification of the viscosity. Thus, only a reduction of the slip length would account for the discrepancy concerning the effective viscosity evidenced in Fig. 5(a). Assuming now that the viscosity remains close to the bulk value, Eq. (1) is finally used to calculate an effective slip length, which now depends on the channel height. It is displayed in Figs. 5(b) and 5(c). Despite important uncertainties, the effective slip length is greatly reduced below the micron scale, by at least 1 order of magnitude. This effect is stronger for the HPAM200k solutions and for the HPAM8M solutions containing 10 g/L of NaCl. The smaller the chain dimension, the bigger the slippage reduction. The results obtained in the presence of salt indicate that this effect should also exist in the case of neutral polymers.

Such a reduction of slip length has been observed in Brownian dynamics [25] or molecular dynamics [26] simulations, and can be interpreted in terms of chain migration. Indeed, migration is coming from hydrodynamic interactions, which are screened in confinement [22,25]. Let us recall that only migration can explain the large thickness of the depletion layer observed in our system. In a large channel, the depletion layer thickness is between 100 and 800 nm, which is of the order of or even bigger than the channel height. Therefore, it is not surprising to find a modification and a reduction of the depletion layer in nanoslits. A distinction between surface and bulk properties is no longer valid. Consequently, the flow of polymer solutions could not be accounted for by macroscopic rheological and slippage properties, even in moderate confinement.

In conclusion, we have taken advantage of both direct measurements of slip lengths of polyelectrolyte solutions in microfluidic channels and characterizations of effective viscosities in nanoslits ranging from 0.1 to a few micrometers to characterize the wall slip at scales smaller than the depletion layer. Although we observe an important reduction of the effective viscosity below 1 μm, this reduction is much lower than expected. This result is interpreted in terms of a reduction of the slip length due to confinement. Since the strong slippage observed is likely to be due to migration away from the wall, this result strongly indicates that the latter is canceled in nanochannels, in agreement with some recent simulations. This work calls for additional theoretical work in order to capture the effects of concentration, chain lengths, and ionic strength. From an experimental standpoint, it would be interesting to measure directly the variation of the depletion layer and to extend both the concentration range and the polymer properties.

The authors thank Région Aquitaine, Rhodia, CNRS, and Carnot Institute Isifor for funding. Samuel Marre is acknowledged for his help concerning the anodic bounding.

*hugues.bodiguel@u-bordeaux1.fr

[1] A. v. d. B. Sparreboom and J. C. T. Eijkel, Nat. Nanotechnol. **4**, 713 (2009).

[2] J. Edel and A. De Mello, *Nanofluidics: Nanoscience and Nanotechnology* (Royal Society of Chemistry, London, 2009).

[3] L. W. Lake, *Enhanced Oil Recovery* (Prentice-Hall, Englewood Cliffs, NJ, 1989).
[4] L. Bocquet and E. Charlaix, Chem. Soc. Rev. **39**, 1073 (2010).
[5] U. S. Agarwal, A. Dutta, and R. A. Mashelkar, Chem. Eng. Sci. **49**, 1693 (1994).
[6] H. A. Barnes, J. Non-Newtonian Fluid Mech. **56**, 221 (1995).
[7] J. Sanchez-Reyes and L. A. Archer, Langmuir **19**, 3304 (2003).
[8] G. Chauveteau, M. Tirrell, and A. Omari, J. Colloid Interface Sci. **100**, 41 (1984).
[9] Y. M. Joshi, A. K. Lele, and R. A. Mashelkar, J. Non-Newtonian Fluid Mech. **89**, 303 (2000).
[10] C. Allain, D. Ausserre, and F. Rondelez, Phys. Rev. Lett. **49**, 1694 (1982).
[11] D. Ausserre, H. Hervet, and F. Rondelez, Macromolecules **19**, 85 (1986).
[12] D. Ausserre, J. Edwards, J. Lecourtier, H. Hervet, and F. Rondelez, Europhys. Lett. **14**, 33 (1991).
[13] L. Fang, H. Hu, and R. G. Larson, J. Rheol. **49**, 127 (2005).
[14] A. Omari, M. Moan, and G. Chauveteau, Rheol. Acta **28**, 520 (1989).
[15] Y. Cohen and A. B. Metzner, J. Rheol. **29**, 67 (1985).
[16] X. J. Fan, N. Phan-Thien, N. T. Yong, X. H. Wu, and D. Xu, Phys. Fluids **15**, 11 (2003).
[17] R. M. Jendrejack, D. C. Schwartz, J. J. de Pablo, and M. D. Graham, J. Chem. Phys. **120**, 2513 (2004).
[18] H. B. Ma and M. D. Graham, Phys. Fluids **17**, 083103 (2005).
[19] R. Khare, M. D. Graham, and J. J. de Pablo, Phys. Rev. Lett. **96**, 224505 (2006).
[20] J. A. Millan, W. Jiang, M. Laradji, and Y. Wang, J. Chem. Phys. **126**, 124905 (2007).
[21] D. Saintillan, E. S. Shaqfeh, and E. Darve, J. Fluid Mech. **557**, 297 (2006).
[22] M. D. Graham, Annu. Rev. Fluid Mech. **43**, 273 (2011).
[23] L. Fang, C. C. Hsieh, and R. G. Larson, Macromolecules **40**, 8490 (2007).
[24] L. Fang and R. G. Larson, Macromolecules **40**, 8784 (2007).
[25] J. P. Hernandez-Ortiz, H. B. Ma, J. J. Pablo, and M. D. Graham, Phys. Fluids **18**, 123101 (2006).
[26] S. C. Kohale and R. Khare, J. Chem. Phys. **130**, 104904 (2009).
[27] P. Abgrall and N. T. Nguyen, Anal. Chem. **80**, 2326 (2008).
[28] A. Cuenca and H. Bodiguel, Lab Chip **12**, 1672 (2012).
[29] A. Al-Hashmi and P. Luckham, Colloids Surf. A **358**, 142 (2010).
[30] A. V. Dobrynin and M. Rubinstein, Prog. Polym. Sci. **30**, 1049 (2005).
[31] See Supplemental Material at http://link.aps.org/supplemental/10.1103/PhysRevLett.110.108304 for details of the rheological properties of the solutions used and for an estimation of chain lengths.
[32] G. Wallis and D. I. Pomerantz, J. Appl. Phys. **40**, 3946 (1969).
[33] M. Madou, *Fundamentals of Microfabrication: The Science of Miniaturization* (CRC Press, Boca Raton, FL, 2002).
[34] L. Beguin, B. Grassl, F. Brochard-Wyart, M. Rakib, and H. Duval, Soft Matter **7**, 96 (2011).